

Experimental evidence for entangled state formation in a system of two coupled flux qubits

A. Izmalkov,^{1,2} M. Grajcar,^{1,3} E. Il'ichev,¹ Th. Wagner,¹ H.-G. Meyer,¹
A. Yu. Smirnov,⁴ M. H. S. Amin,⁴ Alek Maassen van den Brink,⁴ and A. M. Zagoskin^{4,5,y}

¹Institute for Physical High Technology, P.O. Box 100239, D-07702 Jena, Germany

²Moscow Engineering Physics Institute (State University), Kashirskoe шоссе 31, 115409 Moscow, Russia

³Department of Solid State Physics, Comenius University, SK-84248 Bratislava, Slovakia

⁴D-Wave Systems Inc., 320-1985 West Broadway, Vancouver, B.C., V6J 4Y3 Canada

⁵Physics and Astronomy Dept., The University of British Columbia,
6224 Agricultural Rd., Vancouver, B.C., V6T 1Z1 Canada

The low-frequency response of a system of two inductively coupled flux qubits was monitored using the impedance measurement technique (IMT), which allows to directly read out the magnetic susceptibility of the qubits and the curvature of their average energy as a function of external dc magnetic flux. In a single qubit, an IMT dip marks the level anticrossing due to coherent tunneling and allows to determine the tunneling amplitude. In a two-qubit system, the non-zero difference between the sum of single-qubit IMT dips, and the IMT dip amplitude when the qubits are both at a degeneracy point (IMT deficit) shows that the system is in a mixture of entangled two-qubit states (a necessary condition for two-qubit entanglement). The dependence of the IMT dips on temperature and relative bias between the qubits allows to determine all the parameters of the effective Hamiltonian and equilibrium density matrix and confirm the formation of entangled eigenstates.

The demonstration of quantum entanglement in macroscopic systems remains a daunting task even after the successful observation of quantum coherence in many types of superconducting qubits [1, 2, 3, 4, 5, 6] and after the observation of entanglement in charge [2] and current-biased Josephson-junction (CBJJ) [7] qubits, using pulse and spectroscopic techniques respectively.

In this paper we investigate a system of two flux qubits [8] using a different method, which provides a simple criterion for the formation of entangled states.

The IMT method [9] relies on monitoring the current and voltage in a high-quality, low-frequency resonant tank circuit inductively coupled to the qubit and fed a small-amplitude ac signal. The effective impedance of the system, and therefore the current-voltage phase angle in the tank, depend on the qubit state. In various modifications, this method was applied to map the Josephson potential profile [10] and to observe Landau-Zener transitions [11], coherent tunneling [12], and Rabi oscillations [13] in a three-junction flux qubit. Due to the tank's weak coupling to the qubit and high quality factor, the method allows to achieve decoherence times as high as 2.5 ns [13]. It is important to realize that the IMT approach requires that the decoherence rate be small compared to the tunneling amplitudes (0.5–1 GHz), not the tank frequency (10–20 MHz).

The system of two flux qubits inductively coupled to each other and to the tank is shown in Fig. 1. The qubits were fabricated out of aluminum by conventional shadow evaporation, normally 1 μm apart, at the centre of a niobium pickup coil. The area of each qubit and self-inductance, critical current, and Coulomb energy of the junctions were $S_q = 80 \text{ nm}^2$, $L_q = 39 \text{ pH}$,

$I_c = 400 \text{ nA}$, and $E_C = 3.2 \text{ GHz}$, respectively. The mutual inductance between the qubits $M_{ab} = 2.7 \text{ pH}$ was estimated numerically from the electron micrograph. The niobium coil, which together with an external capacitor $C_T = 470 \text{ pF}$ forms a parallel tank circuit with inductance $L_T = 130 \text{ nH}$, resonant frequency $f_T = 1/T = 20.139 \text{ MHz}$ and quality factor $Q_T = 1680$ (at 10 mK), was fabricated using e-beam lithography. The magnetic flux through the qubits was created by the dc component of the current in the coil I_{dc1} , and by the bias current I_{dc2} through a wire close to one of the qubits. This allowed independent control of the bias in each qubit.

The system of Fig. 1 is described by the Hamiltonian $H = H_0 + H_T + H_{int} + H_{diss}$, where the two-qubit Hamiltonian in the two-state approximation is expressed through Pauli matrices as [14]

$$H_0 = \frac{1}{2} \left(\sigma_x^{(a)} \sigma_x^{(b)} + \sigma_z^{(a)} + \sigma_z^{(b)} \right) + J \sigma_z^{(a)} \sigma_z^{(b)}; \quad (1)$$

H_T is the tank Hamiltonian (a harmonic oscillator), the qubit-tank interaction is

$$H_{int} = \left(\sigma_z^{(a)} + \sigma_z^{(b)} \right) I_T; \quad (2)$$

and H_{diss} describes the standard weak coupling of the qubits to a dissipative bath [15].

Here L_T , f_T and I_T are the inductance, resonant frequency and current in the tank, respectively. The coefficients are $\sigma_{a=b} = M_{a=b/T} I_{a=b}$, where $M_{a=b/T}$ is the qubit-tank mutual inductance, $L_{a=b}$ is the self-inductance and $I_{a=b}$ is the amplitude of the persistent current in the corresponding qubit. In the standard two-state approximation, the qubit current operators are $\hat{I}_{a=b} = I_{a=b} \sigma_z^{(a=b)}$. The qubit biases are given by $\phi_a = I_{a=0} (\phi_x - 0.5 + \phi_{shift})$,

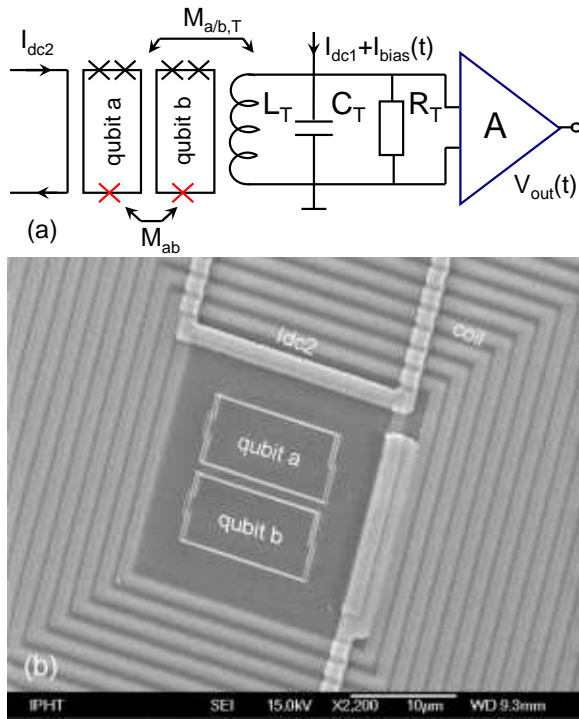


FIG. 1: Two-qubit system coupled to a resonant tank circuit. (a) Schematic of the circuit. (b) Micrograph.

$b = I_b \left(f_x \pm 0.5 + f_{\text{shift}} \right)$, where the dimensionless flux $f_x = \Phi_x / \Phi_{c1}$ describes the field created by the niobium coil in both qubits, while the parameters f_{shift} , Φ_{c2} and $M_{bw} = M_{aw} < 1$ give the bias difference between the qubits created by the additional wire. Here M_{aw} (M_{bw}) are the mutual inductances between the a (b) qubit and the additional dc wire (for our sample, M_{aw} and M_{bw} were calculated numerically, yielding $M_{bw} = 0.32$). The qubit-qubit coupling constant $J = M_{ab} I_a I_b$ is positive because the two qubits are in the same plane side to side, leading to antiferromagnetic coupling (according to the north-to-south attraction law).

The effective inductance of the tank, and therefore its resonant frequency, depends on the state of the qubits. In the framework of the IMT method [9], this shift is observed by continuously monitoring the phase angle between the average tank voltage and time-dependent bias current $I_{\text{bias}}(t)$ fed into the tank (Fig. 1). For small enough I_{bias} , $\tan \delta$ is determined by the real part of the magnetic susceptibility of the two-qubit system $\chi''(\omega_T)$ [17] taken at ω_T , viz., $\tan \delta = 2(Q_T = L_T \omega_T)^{-1} \chi''(\omega_T)$. For a single qubit and zero temperature, $\chi''(\omega_T)$ and $\tan \delta$ are proportional to the second derivative of the qubit ground-state energy with respect to the tank flux $\Phi_T = L_T I_T$. In the linear-response approximation, the magnetic susceptibility of the two-qubit system $\chi''(\omega)$ is expressed through retarded Green's functions of the qubit operators $S_z^{(a=b)}$, calculated with the equilibrium density matrix $\rho = e^{-(H_0 - \Phi_0)} / Z$ with H_0 as in

Eq. (1). It can be generally assumed that the latter's eigenvalues E_j , $j = 1; 2; 3; 4$, are non-degenerate and the eigenstates are orthonormalized, $\langle j | i \rangle = \delta_{ji}$. Taking into account the qubits' interaction with a dissipative environment [16, 17], we derive [18]

$$\chi''(\omega) = \frac{\chi''(\omega)}{\epsilon} \frac{R}{\omega^2 + E_j^2 + \Gamma_j^2} ; \quad (3)$$

$$\tan \delta = 4 \frac{Q_T}{L_T} \frac{\chi''(\omega)}{\omega} \frac{R}{E_j^2 + \Gamma_j^2} ; \quad (4)$$

where $Z_j = \exp(-E_j/T) / Z$ is a thermal population of the energy level, $Z = \sum_j \exp(-E_j/T)$; Γ_j are decoherence rates of the double-qubit system, and

$$\begin{aligned} \chi''(\omega) = & \frac{2}{a} h \langle j_z^{(a)} \rangle \langle j_z^{(a)} \rangle + \frac{2}{b} h \langle j_z^{(b)} \rangle \langle j_z^{(b)} \rangle \\ & + \frac{2}{a} h \langle j_z^{(a)} \rangle \langle j_z^{(b)} \rangle \\ & + \frac{2}{a} h \langle j_z^{(b)} \rangle \langle j_z^{(a)} \rangle ; \end{aligned} \quad (5)$$

At low frequencies $\omega \ll \omega_T \ll E_j$ and in a weak damping regime $\Gamma_j \ll E_j$, the decoherence rates have no effect on $\tan \delta$, but are responsible for the establishment of the equilibrium distribution in the system.

The first two terms in Eq. (5) are non-zero even if the two-qubit states are factorized. The first (second) term corresponds to the contribution of qubit a (b), and is nonzero near that qubit's degeneracy point. These contributions are practically independent of whether the qubits' degeneracy points coincide or not.

The second line in Eq. (5) describes coherent flipping of both qubits, which is only possible for non-factorizable (entangled) eigenstates $|j_i, j_i\rangle$. Therefore the difference between the coinciding IMT dip of the two qubits and the sum of two single-qubit IMT dips provides a measure of how coherent is the two-qubit dynamics [that is, whether entangled eigenstates of the two-qubit Hamiltonian Eq. (1) are formed]. This is a necessary condition for the system to be in an entangled (pure or mixed) state.

The measurements in our system of Fig. 1 allowed to determine all the parameters of the Hamiltonian (1). The experimental data are presented in Fig. 2 ($\tan \delta$ vs. external flux bias at 10, 50, 90 and 160 mK) and Fig. 4 (temperature dependence of IMT dip amplitudes).

First, we match the single-qubit IMT dips of Fig. 2 [with $I_{dc2} = 27.3$ (± 3.7) A, i.e. in the regime when the qubits are separated in biases] with the theoretical predictions of Eqs. (4), (5) (see Fig. 3). This yields the values $I_a = 550$ MHz, $I_b = 450$ MHz. The width of the IMT dip is practically temperature-independent, as expected [12].

Then, the temperature dependence of the single-qubit dips (Fig. 4, squares and triangles) allows to determine the amplitude of the persistent current: $I_a = I_b =$

$I_p = 320$ nA, which corresponds to the energy scale $I_p \Phi_0 = 990$ GHz. (The saturation below 35{40 mK is likely due to the discrepancy between the nominal temperature of the mixing chamber and the temperature of the sample. The same saturation temperature was observed in Ref. [12].)

We can determine the coupling constant J in Eq. (1) from the single-qubit measurements, using the value of the persistent current I_p and the mutual inductance between the qubits, $M_{ab} = 2.7$ pH calculated from the electron micrograph (Fig. 1b). Then $J = M_{ab} I_p^2 = 410$ MHz. This value agrees well with the value $J = 420$ MHz, obtained by fitting the temperature dependence of the coincident IMT dip amplitude above the saturation temperature (Fig. 4, circles) with the theoretical curve.

Comparison of the single-qubit dips with the coincident IMT dip shows clearly that the contribution to $\tan \delta$ from the entangled eigenstates is significant. Indeed, the amplitude of the central dip in Fig. 2 at $T = 50$ mK is 1.12, compared to the sum of the single qubit dips equal to 1.69. It means that the entangled terms [second line in Eq. (5)] are responsible for the negative contribution

0.57 to $\tan \delta$. Alternatively, one can calculate the coincident IMT dip dropping the contributions from the entangled states in Eq. (5) (dotted line in Fig. 3). The difference is as spectacular.

Note that the IMT deficit also confirms the sign of the qubit-qubit interaction: in the case of ferromagnetic coupling the sum of the single-qubit dips should be less than the coincident one.

Plotting the ratio of the coincident dip to the average single-qubit dip (Fig. 4, inset), we see that it grows with temperature and approaches 2. This is to be expected: thermal excitations tend to destroy coherent correlations between the qubits, which will lead to qubits behaving as independent quantum systems (with zero IMT deficit), and then, of course, destroy the single-qubit IMT dips as well.

At 50 mK the temperature is comparable to the characteristic energies in the two-qubit system (at the two-qubit degeneracy point the gap between the ground state and top excited state is 100 mK). Since the characteristic measurement time in our approach is dictated by the much smaller tank frequency, ω_T , the system will have time to equilibrate. Indeed, an excellent quantitative agreement between the experiment in a wide range of temperatures (Fig. 3, 4) and the theory Eq. (4) confirms that the system is described by the equilibrium density matrix with the Hamiltonian Eq. (1) (all the parameters of which we determined from the experiment). In other words, our system is in an equilibrium mixture of entangled two-qubit states.

An entanglement measure of a system in an arbitrary state (the concurrence C [19], changing monotonically from 0 for non-entangled to 1 for a maximally entangled state) depends both on the existence of entangled

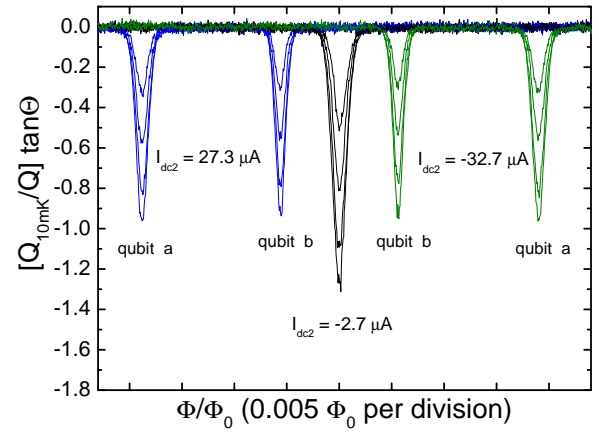


FIG. 2: Normalized tangent of the current-voltage angle in the tank as a function of the external bias $f_x = 0$. From the lower to upper curves the temperature of the mixing chamber is 10, 50, 90, 160 mK. Relative flux bias f_{shift} between the qubits is created by changing the current I_{dc2} in the additional wire. The shifted curves correspond to $I_{dc2} = 27.3$ (-32.7) A. Two IMT dips are observed, showing tunneling splitting in each qubit at the corresponding degeneracy point $f_x \notin 0.5$. The central curve: $I_{dc2} = 2.7$ A. Both qubits are degenerate simultaneously at $f_x = 0.5$. One IMT dip is observed, with the amplitude about 33% (at small temperatures) less than the sum of two separate dips.

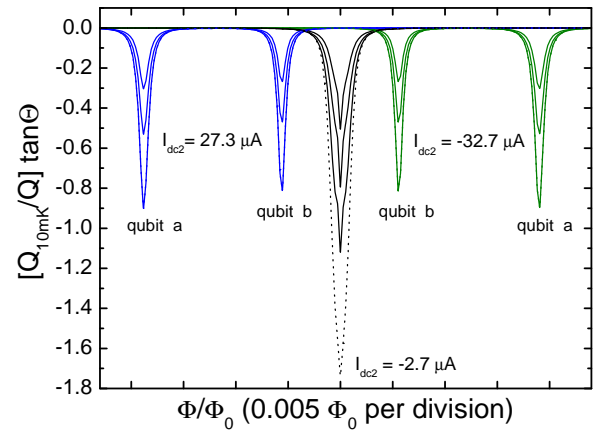


FIG. 3: Theoretical fitting of normalized tangent of the current-voltage angle in the tank as a function of the external bias $f_x = 0$. Solid curves: from the lower to upper curves the temperature takes values 50, 90, 160 mK. Interaction energy between two qubits is 420 MHz. A dotted curve corresponds to $J = 420$ MHz and $T = 50$ mK, with the contributions from the entangled eigenstates in (5) omitted. Relative flux biases are taken the same as for experimental curves, see Fig. 2.

eigenstates and on their population, and can be erased by temperature faster than quantum coherence in individual qubits [20].

Using the experimentally established parameters of the Hamiltonian (1), the concurrences of its eigenstates at the two-qubit degeneracy point are immediately calcu-

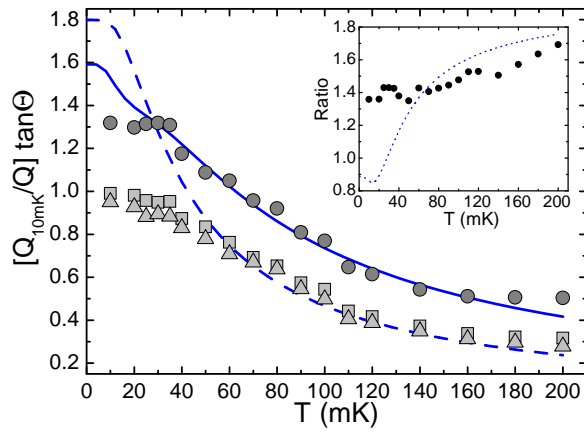


FIG. 4: Temperature dependence of the IMT dip amplitudes. Squares: qubit a, triangles: qubit b. Circles: coincident IMT dip amplitude. The solid and dashed curves correspond to theoretical fitting. Inset: relative size of the coincident IMT dip. Ratio is $2 \tan \theta_c = (\tan \theta_a + \tan \theta_b)$; the dotted line is the theoretical curve.

lated: $C_1 = C_4 = 0.39$, $C_2 = C_3 = 0.97$. For the equilibrium density matrix of our system at 10 mK, these give $C_{eq} = 0.33$. This value will decrease with rising temperature, vanishing around 30 mK.

We must stress, that for the quantum computing applications, it is the existence of entangled eigenstates of two qubits that matters, not the measure of equilibrium entanglement, since then the system anyway must operate on a faster scale than the time of equilibration. The crucial requirement here is that the decoherence time τ_{2q} of the entangled eigenstates exceeds the operation time. The fact of observation of the IMT dips and IMT deficit indicates that in our system τ_{2q} is larger than $\tau_{in}(l_{a=b}, l=J) \approx 1$ ns; its actual value can be determined using the approach of [13].

In conclusion, we investigated the system of two inductively coupled aluminum flux qubits with independent control over biasing fluxes. We used the impedance mea-

surement technique, which directly measure the low frequency part of the magnetic susceptibility of the system and produces a snapshot of the curvature of its average energy as a function of external magnetic flux.

The excellent quantitative agreement between the theoretical predictions and the experimental data confirms that the system is in an equilibrium mixture of entangled two-qubit states.

We thank N. Oukhanski, H. Mühlig, D. Born for technical assistance, U. Hubner and T. May for sample fabrication and I. Aeck, D. Bonn, M. Franz, W. Hardy, P. C. E. Stamp, M. F. H. Steiner, and H. E. Hoening for fruitful discussions.

Electronic address: ilichev@ipht-jena.de

^y Electronic address: zagoskin@dwavesys.com

- [1] Y. Nakamura, Yu. A. Pashkin, and J. S. Tsai, Nature 398, 786 (1999).
- [2] Yu. A. Pashkin et al., Nature 421, 823 (2003).
- [3] J. R. Friedman et al., Nature 406, 43 (2000).
- [4] J. E. Mooij et al., Science 285, 1036 (1999).
- [5] J. M. Martinis et al., Phys. Rev. Lett. 89, 117901 (2002).
- [6] D. Vion et al., Science 296, 886 (2002).
- [7] A. J. Berkley et al., Science 300, 1548 (2003).
- [8] J. B. Majer et al., cond-mat/0308192.
- [9] Ya. S. Greenberg et al. Phys. Rev. B 66, 214525 (2002).
- [10] E. Il'ichev et al., Appl. Phys. Lett. 80, 4184 (2002).
- [11] A. Izmailkov et al., cond-mat/0307506.
- [12] M. G. Rajjar et al., cond-mat/0303657 (to appear in Phys. Rev. B Rapids).
- [13] E. Il'ichev et al., Phys. Rev. Lett. 91, 097906 (2003).
- [14] A. M. Aassen van den Brink, cond-mat/0310425.
- [15] U. Weiss, Quantum Dissipative Systems, 2nd edition (World Scientific, Singapore, 1999).
- [16] K. Blum, Density matrix theory and applications (Plenum Press, New York, 1981).
- [17] A. Yu. Smirnov, Phys. Rev. B 68, 134514 (2003).
- [18] A. Yu. Smirnov, unpublished.
- [19] W. K. Wootters, Phys. Rev. Lett. 80, 2245 (1998).
- [20] T. Yu and J. H. Eberly, Phys. Rev. B 66, 193306 (2002).